J. Fluid Mech. (2005), *vol.* 526, *pp.* 147–170.
DOI: 10.1017/S0022112004002782 Printed in the United Kingdom

On the growth (and suppression) of very short-scale disturbances in mixed forced–free convection boundary layers

By JAMES P. DENIER[1], PETER W. DUCK[2] AND JIAN LI[1]

[1]School of Mathematical Sciences, The University of Adelaide, South Australia, 5005, Australia

[2]Department of Mathematics, The University of Manchester, Oxford Road, Manchester, M13 9PL, UK

(Received 9 December 2003 and in revised form 1 October 2004)

The two-dimensional boundary-layer flow over a cooled/heated flat plate is investigated. A cooled plate (with a free-stream flow and wall temperature distribution which admit similarity solutions) is shown to support non-modal disturbances, which grow algebraically with distance downstream from the leading edge of the plate. In a number of flow regimes, these modes have diminishingly small wavelength, which may be studied in detail using asymptotic analysis.

Corresponding non-self-similar solutions are also investigated. It is found that there are important regimes in which if the temperature of the plate varies (in such a way as to break self-similarity), then standard numerical schemes exhibit a breakdown at a finite distance downstream. This breakdown is analysed, and shown to be related to very short-scale disturbance modes, which manifest themselves in the spontaneous formation of an essential singularity at a finite downstream location. We show how these difficulties can be overcome by treating the problem in a quasi-elliptic manner, in particular by prescribing suitable downstream (in addition to upstream) boundary conditions.

1. Introduction

Mixed forced–free convection boundary layers have been much studied in the past due to their importance in a wide variety of heat transfer applications in industry. There is now a considerable body of literature on this class of flow which can be divided into studies on heat transfer (Leal 1973; Hady, Bakier & Gorla 1996), flow stability (Chen & Mucoglu 1979; Denier & Bassom 2003; Denier & Mureithi 1996) and critical phenomena associated with the breakdown of the boundary-layer approximation (Daniels 1992; Daniels & Gargaro 1993; Schneider 1979; Schneider & Wasel 1985).

Much of the work on this class of flows can be viewed as studies into the effect of buoyancy upon the behaviour of the boundary-layer flow. The effect of buoyancy upon heat transfer in mixed convection boundary layers has been considered by a number of authors. Hady *et al.* (1996) demonstrated that incorporating a temperature dependency into the model has a significant effect on the heat transfer and (laminar) drag characteristics of the flow. Importantly a velocity overshoot, in which the streamwise velocity exceeds the free-stream velocity, was observed at sufficiently high levels of buoyancy. Leal (1973) considered the general problem of a mixed convection

boundary layer over a flat plate inclined at an angle to the horizontal. Similarity solutions were developed as series expansions in powers of a (small) buoyancy parameter. A number of asymptotic limits, based upon the magnitude of the Prandtl number, were investigated in the context of quantifying the effect of buoyancy on skin friction and heat flux at the plate surface. Hussain & Afzal (1988) employed a higher-order expansion method, similar to that used by Leal (1973), to further refine predictions of heat transfer and drag characteristics for mixed convection flows.

All the aforementioned works were based upon the concept of similarity (or local similarity) of the mixed convection boundary layer. Under conditions of a uniform free-stream speed and a uniform plate temperature (or a constant heat flux at the wall) similar solutions are no longer possible. Then the full parabolic partial differential equations must be solved and this calculation was first undertaken by Schneider & Wasel (1985). Their results showed that in the case of a unstably stratified flow, the streamwise velocity develops an overshoot at a given streamwise location. Interestingly, a stably stratified flow (corresponding to, for example, a cooled wall) terminates in a singularity that is not directly associated with boundary-layer separation. Schneider & Wasel (1985) attribute this singularity to the presence of a local turning point in the wall shear. This argument is not entirely convincing since it ignores the important point that the local turning point is intimately linked to the non-uniqueness of self-similar solutions (as we will show in § 3), a point overlooked by Schneider (1979) in his study on self-similar flows.

Steinrück (1994) investigated the boundary-layer flow over a cooled horizontal plate, and found numerical difficulties that were associated with large eigenvalues associated with perturbations to the flow field. His analysis (which may be regarded as being linked to one particular choice of parameters in our analysis) was based on the use of modal flow disturbances and consequently involved the use of the parallel-flow approximation; as such the approach was largely heuristic. In the present paper, in addition to studying a much wider class of problem, the analysis for the most part is completely rigorous, mathematically, and we show that even heated-flow situations can be susceptible to numerical difficulties. We also present a resolution of these difficulties, using a somewhat novel approach.

In addition to the purely flat-plate mixed convection flow, velocity overshoot occurs in a variety of other important problems. Kumari & Nath (1982) demonstrated streamwise velocity overshoot in three-dimensional stagnation-point flows; the characteristics of the flow being similar to the flat-plate analogue. A similar phenomenon can be found in the work of Daniels & Gargaro (1993) where the flow has a stable thermal stratification but the overshoot is due to the intrusion of a non-buoyant wall jet. In this case the velocity overshoot vanishes as the flow develops in the streamwise direction (see their figure 6); this is in direct contrast to the unstably stratified mixed convection flow for which the strength (or magnitude) of the velocity overshoot increases with increasing distance from the leading edge of the plate.

It is inevitable that whenever an overshooting-type situation arises, the underlying boundary-layer profile becomes inflectional and therefore inviscidly unstable. The linear stability of a particular family of self-similar buoyant boundary layers was considered by Mureithi, Denier & Stott (1997) who demonstrated that the flow, when subject to wave-like disturbances, develops a 'degenerate' critical layer at the position where the streamwise velocity attains its maximum. It was shown that these modes are short compared with the boundary-layer thickness and that they propagate downstream with a wave speed equal to the maximum value of the mean streamwise velocity. The analysis was extended into the weakly nonlinear regime by Denier &

Mureithi (1996) who uncovered a supercritical bifurcation to a new class of finite-amplitude travelling waves. These are governed by a mean-field theory in which the fundamental component of the disturbance is coupled to the mean-flow correction induced by the self-interaction of the fundamental itself. Further work on the stability of the flow to $O(1)$-wavelength disturbances can be found in Chen & Mucoglu (1979) and Mureithi (1998). Chen & Mucoglu (1979) employed a parallel-flow approximation to pose the problem of the wave instability of the flow in terms of a generalized Orr–Sommerfeld equation coupled through the buoyancy term to a disturbance energy equation. Curves of neutral stability demonstrated that the effect of buoyancy is to destabilize the flow, although multiple modes of instability were also uncovered. These new modes led to predicted critical Reynolds number (based upon a characteristic length) of $O(10)$. Further work on this problem is in Mureithi (1998), where a variety of unstable modes were found – again these have the property that instability arises at values of the Reynolds number in the range $O(10)$. However, their relevance to true boundary-layer flows, for which the Reynolds number is large, is not clear. The effect of non-parallelism on this class of instability has recently been considered by Denier & Bassom (2003), where it was shown that nonlinear short waves become increasingly focused within the degenerate critical layer as the flow develops in the streamwise direction. Stability aspects of the related natural convection problem have also been the subject of investigation – see for example Higuerra (1992).

To date, with the exception of Steinrück (1994), all results concerning the stability of mixed forced–free convection boundary layers have focused upon wave-like (normal mode) disturbances. Recently, however, there has been renewed interest in the problem of non-modal disturbances in boundary-layer flows, a problem first studied by Libby & Fox (1964). Luchini (1996) considered the instability of a flat-plate boundary layer to three-dimensional non-modal (in the streamwise direction) disturbances. Such disturbances are ascribed to the interplay between inviscid algebraic growth and viscous dissipation and it is demonstrated that, although viscous dissipation provides an algebraic decay it is unable to overcome the inviscid algebraic growth. This is in stark contrast to the equivalent problem in a parallel flow where algebraic decay resulting from viscous dissipation does serve to damp out the inviscid algebraic growth, thus resulting in a flow which is stable to such disturbances. The existence of algebraically growing disturbances (within the context of the boundary-layer flow) provides a driving mechanism for the linear amplification stage observed in experiments on by-pass transition. Luchini (2000) extended this work to consider the question of optimal disturbances within the boundary-layer flow, thus strengthening the link between algebraic disturbances and by-pass transition (for further discussion on algebraically growing disturbances see Andersson, Berggren & Henningson (1999) and Obrist & Schmid (2003) for spatial growth and Trefethen *et al.* (1993) for temporal growth).

Here we are concerned with the Reynolds-number independent instability of a class of mixed forced–free convection boundary-layer flows. The problem is formulated in § 2. Basic similarity flows are considered in § 3, where for cooled flows (that is, the surface temperature is less than the free-stream temperature) the self-similar flow is non-unique. The instability of these self-similar flows to algebraically growing disturbances is demonstrated numerically. Sections 3.1 and 3.2 describe the asymptotic form of the disturbance for large disturbance growth rate, thus confirming our numerical results. In § 4 we turn our attention to the non-parallel evolution of the boundary layer where we demonstrate the existence of a very short-scale instability. Finally in § 5 we show that the instabilities described in previous sections can be

suppressed through a quasi-elliptic treatment of the boundary-layer flow. Some conclusions from our study are drawn in § 6.

2. Formulation

The dimensionless equations which govern the two-dimensional motion of a steady incompressible Boussinesq fluid flowing over a heated/cooled flat plate may be written in the form

$$\frac{\partial \tilde{u}}{\partial x} + \frac{\partial \tilde{v}}{\partial y} = 0, \tag{2.1a}$$

$$\tilde{u}\frac{\partial \tilde{u}}{\partial x} + \tilde{v}\frac{\partial \tilde{u}}{\partial y} = -\frac{\partial \tilde{p}}{\partial x} + \frac{1}{Re}\nabla^2\tilde{u}, \tag{2.1b}$$

$$\tilde{u}\frac{\partial \tilde{v}}{\partial x} + \tilde{v}\frac{\partial \tilde{v}}{\partial y} = -\frac{\partial \tilde{p}}{\partial y} + G\tilde{T} + \frac{1}{Re}\nabla^2\tilde{v}, \tag{2.1c}$$

$$\tilde{u}\frac{\partial \tilde{T}}{\partial x} + \tilde{v}\frac{\partial \tilde{T}}{\partial y} = \frac{1}{\sigma Re}\nabla^2\tilde{T}, \tag{2.1d}$$

where $\nabla^2 \equiv \partial^2/\partial x^2 + \partial^2/\partial y^2$. Here the fluid velocities have been scaled on a typical free-stream speed U_∞ and the distances along (x) and normal to (y) the plate expressed relative to a characteristic length L. The pressure $\tilde{p}$ has been non-dimensionalized using $\rho_0 U_\infty^2$ where ρ_0 is the density of the fluid at the temperature of the plate (T_0) and the fluid temperature $\tilde{T}$ has been written relative to the difference $T_0 - T_\infty$ where T_∞ is the temperature of the free stream. The Prandtl number is denoted by σ and the Reynolds number Re takes its usual form equal to $U_\infty L/\nu$ where ν represents the kinematic viscosity of the fluid. Lastly, within (2.1) we have defined $G = GrRe^{-2}$ where $Gr = g\beta L^3(T_0 - T_\infty)/\nu^2$ is the Grashof number; g denotes the acceleration due to gravity, and β is the coefficient of volume expansion.

When $Re \gg 1$ the velocity, pressure and temperature fields within the boundary layer can be written as

$$(\tilde{u}, \tilde{v}, \tilde{T}, \tilde{p}) = \left(u, Re^{-1/2}v, T, -\tfrac{1}{2}u_e^2(x) + Re^{-1/2}p\right) + \cdots, \tag{2.2}$$

where the quantities on the right-hand side are functions of x and the boundary-layer variable $Y \equiv Re^{-1/2}y$. The governing equations then become (to leading order in powers of Re)

$$\frac{\partial u}{\partial x} + \frac{\partial v}{\partial Y} = 0, \tag{2.3a}$$

$$u\frac{\partial u}{\partial x} + v\frac{\partial \bar{u}}{\partial Y} = u_e\frac{\mathrm{d}u_e}{\mathrm{d}x} - G_0\frac{\partial p}{\partial x} + \frac{\partial^2 u}{\partial Y^2}, \tag{2.3b}$$

$$\frac{\partial p}{\partial Y} = T, \tag{2.3c}$$

$$u\frac{\partial T}{\partial x} + v\frac{\partial T}{\partial Y} = \frac{1}{\sigma}\frac{\partial^2 T}{\partial Y^2}, \tag{2.3d}$$

subject to the boundary conditions $u = v = 0$, $T = T_w(x)$ on the plate $Y = 0$ and that $u \to u_e(x)$, $T \to 0$ as $Y \to \infty$. In (2.3), the apparently small term $G_0 \equiv Re^{-1/2}G$ has been retained and the pressure has been rescaled using G_0. The extreme cases in which $G_0 \ll 1$ or $G_0 \gg 1$ are respectively referred to as forced and free convection boundary layers, whereas our interest here is in the intermediate regime for which $G_0 = O(1)$. Then the momentum and temperature fields within the boundary layer

become fully coupled and this provides a mechanism whereby the buoyancy-induced streamwise pressure gradient can serve to accelerate the streamwise flow to levels above its normalized free-stream speed.

Before proceeding it is worthwhile to note estimates that characterize some of the key parameters involved. For example, water at 20° C has kinematic viscosity $\nu = 1.004 \times 10^{-2}$ cm^2 s^{-1} and coefficient of thermal expansion $\beta = 2.1 \times 10^{-4}$ K^{-1} (see Batchelor 1967). If we consider a device in which the characteristic length scale L is, say, 100 cm and the temperature difference ΔT is 20° C then the Grashof number $Gr \sim O(10^{10})$. If the water is replaced by air then Gr drops by up to roughly two orders of magnitude but overall this implies that the $G_0 = O(1)$ regime will be achieved when the associated Reynolds number becomes $O(10^3)$–$O(10^4)$. Such values are readily achieved under controlled experimental conditions (see Wang 1982; Lin & Lin 1996).

We consider a general similarity-like solution to the boundary-layer equations (2.3) by setting

$$\left.\begin{aligned} u &= x^m f'(\eta, x), \qquad v = -\frac{1}{\sqrt{2}}\left((m+1)x^{(m-1)/2} f + (1-m)\eta x^{(m-1)/2} f' - 2x^{(m+1)/2} f_x\right), \\ T &= x^{(5m-1)/2} g(\eta, x), \qquad p = x^{2m} q(\eta, x), \end{aligned}\right\} \tag{2.4}$$

where we have set $u_e = x^m$, $T_w = x^{(5m-1)/2} T_w(x)$. The 'similarity' variable is given by

$$\eta = \frac{Y}{\sqrt{2} x^{(1-m)/2}}. \tag{2.5}$$

Under this transformation the boundary-layer equations become

$$f''' + 2m(1 - (f')^2) + (m+1) f f'' = G_0 \left(4mq + (m-1)\eta q' + 2x \frac{\partial q}{\partial x}\right) + 2x \left(f' \frac{\partial f'}{\partial x} - f'' \frac{\partial f}{\partial x}\right), \tag{2.6a}$$

$$\frac{1}{\sigma} g'' - (5m-1) g f' + (m+1) f g' = 2x \left(f' \frac{\partial g}{\partial x} - g' \frac{\partial f}{\partial x}\right), \tag{2.6b}$$

$$q' = \sqrt{2} g, \tag{2.6c}$$

where a prime denotes differentiation with respect to η. This system must be solved subject to the boundary conditions

$$f = 0, \qquad f' = 0, \qquad g = T_w(x) \quad \text{on} \quad \eta = 0, \tag{2.7}$$

$$f' \to 1, \qquad g \to 0, \qquad q \to 0 \quad \text{as} \quad \eta \to \infty. \tag{2.8}$$

Note that although we have introduced similarity-like variables, this certainly does not preclude us from studying non-similarity-type flows. Indeed, the latter are an important component of this work. However, since the spatial development of the solution will, close to the leading edge, $x = 0$, take on a locally similar form, the variables introduced above enable us to progress the solution downstream in an entirely regular manner.

Finally we note that Steinrück (1994) studied flows which were related to the particular case $m = 0$, $G_0 = 0$ (in our notation).

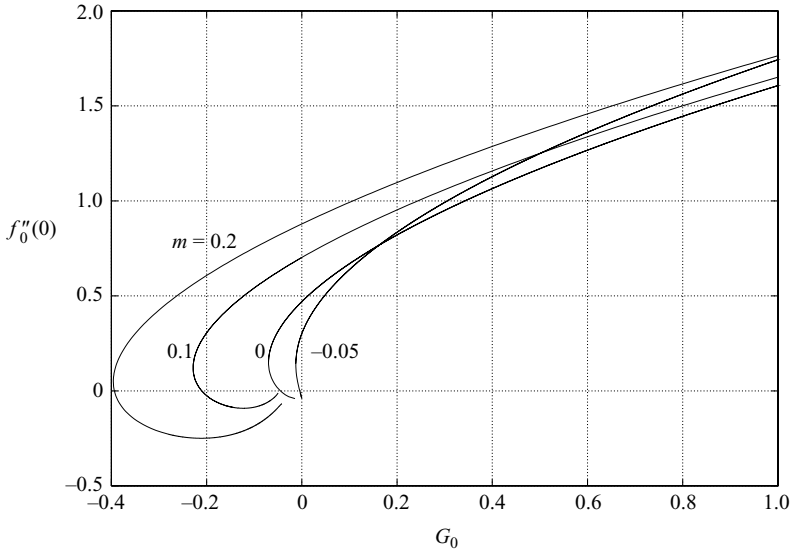

FIGURE 1. Variation of $f_0''(0)$ with G_0.

3. Similarity flows

In this section we study first the form of similarity solutions of (2.6), and then a particular class of disturbance to these base flows. The basic, similarity forms (denoted here by $f_0(\eta)$, $g_0(\eta)$, $q_0(\eta)$) may be obtained from (2.6) by merely setting $x = 0$, leading to

$$f_0''' + 2m(1 - (f_0')^2) + (m+1) f_0 f_0'' = G_0(4mq_0 + (m-1)\eta q_0'), \tag{3.1a}$$

$$\frac{1}{\sigma} g_0'' - (5m-1) g_0 f_0' + (m+1) f_0 g_0' = 0, \tag{3.1b}$$

$$q_0' = \sqrt{2} g_0, \tag{3.1c}$$

which are to be solved subject to the boundary conditions

$$f_0 = 0, \qquad f_0' = 0, \qquad g_0 = 1 \quad \text{on} \quad \eta = 0,$$
$$f_0' \to 1, \qquad g_0 \to 0, \qquad q_0 \to 0 \quad \text{as} \quad \eta \to \infty.$$

This system was solved using a straightforward fourth-order Runge–Kutta technique (coupled with Newton iteration), and results for $m = -0.05$, 0, 0.1 and 0.2, over a range of G_0 are shown in figures 1 and 2 ($f_{00}''(0)$ and $g_{00}'(0)$ respectively). Note that all results shown in this paper were obtained with a Prandtl number $\sigma = 0.72$. These base-flow (similarity) results are reminiscent of the well-known Hartree (1937) distributions encountered in classical Falkner–Skan distributions of wall shear versus Hartree parameter (effectively our parameter m), in which non-uniqueness is found at negative values of the Hartree parameter. In particular, note that the non-uniqueness in the solution for negative values of G_0 mimics the non-uniqueness of the classical Falkner–Skan equations found for negative values of the Hartree parameter. Figure 1 fills in the missing part of the picture presented in Schneider (1979) past the turning point in the wall shear. We note that for $G_0 < 0$ (that is, for flow over a cooled wall) there is the possibility of having two self-similar solutions of the boundary-layer equations, both of which exhibit positive wall shear. It should be noted that these results appear to agree with those of Schneider (1979) when $m = 0$.

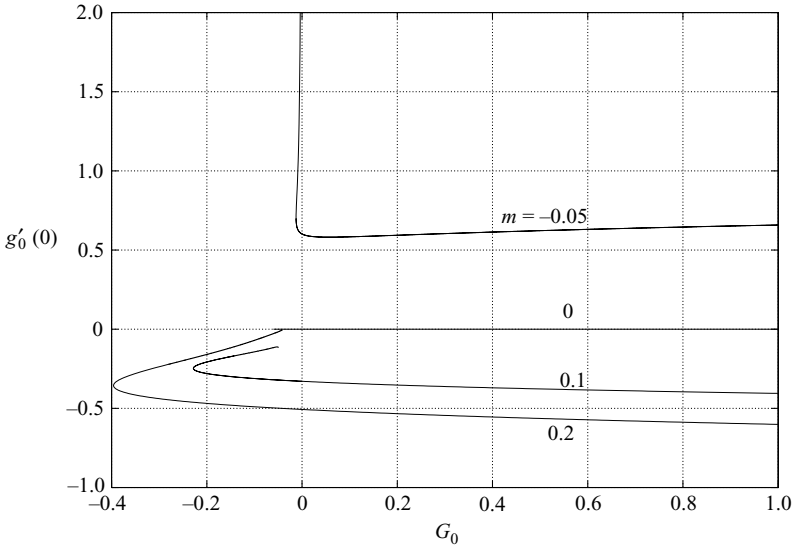

FIGURE 2. Variation of $g_0'(0)$ with G_0 (note that $g_0'(0) \equiv 0$ when $m = 0$).

We next move on to consider stability issues related to these similarity solutions; certainly the occurrence of non-uniqueness raises the question of stability, and is therefore worthy of investigation. At this point it should be noted that the system (2.6) does admit (in a fully rational sense) small-amplitude perturbations which have an algebraic behaviour in the streamwise (x) direction, basically of the same form as that employed by Luchini (1996) and Duck, Stow & Dhanak (1999) in their work on classical boundary layers. In particular we consider perturbations to the basic boundary-layer flow of the form

$$(f, g, q) = (f_0(\eta), g_0(\eta), q_0(\eta)) + x^{\lambda}(f_1(\eta), g_1(\eta), q_1(\eta)) + O(x^{2\lambda}), \tag{3.2}$$

where it is implicitly assumed that $x \ll 1$. Note that the leading-order terms in this expansion are functions of η alone; this is only appropriate if T_w is constant and so we will, without loss of generality, set $T_w = 1$ for the remainder of this section.

Taking the $O(x^{\lambda})$ terms when (3.2) is substituted into (2.6) we obtain

$$f_1''' + (m+1) f_0 f_1'' - 2(2m+\lambda) f_0' f_1' + (m+1+2\lambda) f_1 f_0'' = G_0(2(2m+\lambda) q_1 + (m-1)\eta q_1'), \tag{3.3a}$$

$$\frac{1}{\sigma} g_1'' - (5m-1+2\lambda) g_1 f_0' + (m+1) f_0 g_1' = -(m+1+2\lambda) f_1 g_0' + (5m-1) g_0 f_1', \tag{3.3b}$$

$$q_1' = \sqrt{2} g_1, \tag{3.3c}$$

which are subject to the homogeneous boundary conditions

$$f_1 = 0, \qquad f_1' = 0, \qquad g_1 = 0 \quad \text{on} \quad \eta = 0, \tag{3.4a}$$

$$f_1' \to 0, \qquad g_1 \to 0, \qquad q_1 \to 0 \quad \text{as} \quad \eta \to \infty. \tag{3.4b}$$

This system represents an eigenvalue problem for λ as a function of G_0 (and the Prandtl number σ), which was solved by discretizing all η-derivatives using second-order centred differences. The resulting discretized system can then be written as a

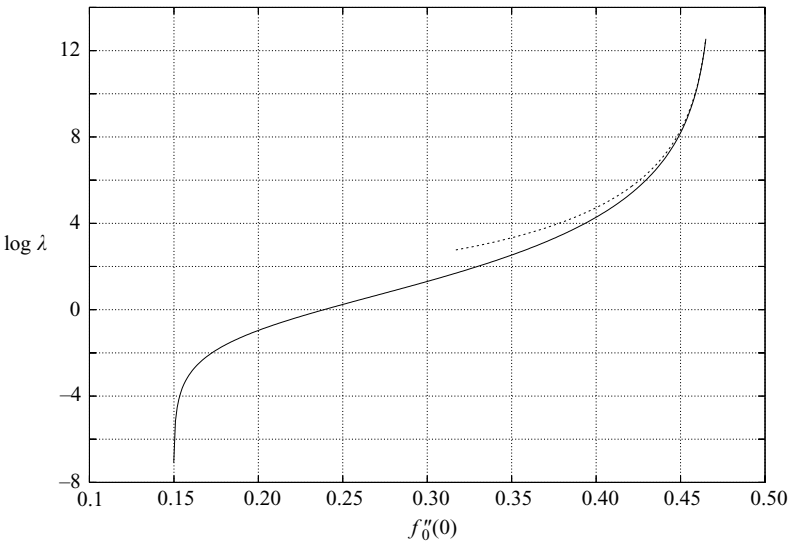

FIGURE 3. The positive eigenvalue for $m = 0$ (asymptotic values shown as broken line).

generalised eigenvalue problem of the form $A\boldsymbol{h} = \lambda B\boldsymbol{h}$ where the vector $\boldsymbol{h}$ contains the field variables at the grid points $\eta_j = j\Delta\eta$. This was then solved, first by using the QZ algorithm to identify estimates for the eigenvalues λ, which were subsequently refined by using the same differencing scheme, but employing a searching (iterative) procedure which exploited the banded nature of the resulting algebraic system. In all the cases (i.e. for all values of the pressure gradient parameter m) studied, for heated boundary layers, namely $G_0 > 0$, only negative values for λ were found, which, in the context of the present paper are of limited interest, although these are of relevance in the far-downstream behaviour of flow disturbances, in the sense of Libby & Fox (1964). It is worth noting in this respect that for the $m = 0$ case, as $G_0 \to 0+$, in addition to the modes found by Libby & Fox (1964) for the Blasius boundary layer, other eigenvalues were found which may be regarded as eigenvalues of the energy equation, one of which was of smaller magnitude ($\lambda \approx -0.296$) than the least negative Libby & Fox (1964) eigenvalue ($\lambda = -1$). It would be the former eigenvalue that controls the downstream decay of the solution.

For the reasons detailed above, we focus on results in regimes which *do* admit positive values of the eigenvalue λ, and therefore flows which admit downstream algebraically growing disturbances. Figure 3 presents results for the case $m = 0$, in particular distributions of (the logarithm of) λ are shown as a function of the wall shear (for later cases, this turns out to be advantageous, rather than as a function of G_0, given the aforementioned non-uniqueness). In this case just one (real) positive eigenvalue was found over the range shown, and the following are the key observations: (i) as $G_0 \to 0-$, $\lambda \to \infty$; (ii) as the 'nose' of the $f_0''(0)$ versus G_0 curve is approached, i.e. as $G_0 \to -0.0699\ldots$, $f''(0) \to 0.149\ldots$, then $\lambda \to 0$; (iii) for the lower branch solution, i.e. for $0.149\ldots < f_0''(0) < 0$, only negative values of λ were encountered; (iv) for $f_0''(0) < 0$ (that is, for reversed flow solutions) a large (probably infinite) number of positive values of λ were encountered (these are not shown); (v) the vast majority of eigenvalues were real. Note that (i) will be considered in detail below, (ii) is an inevitable consequence of the non-uniqueness, whilst (iv) is a reflection of the 'ellipticity' of the flow in the case of flow reversal.

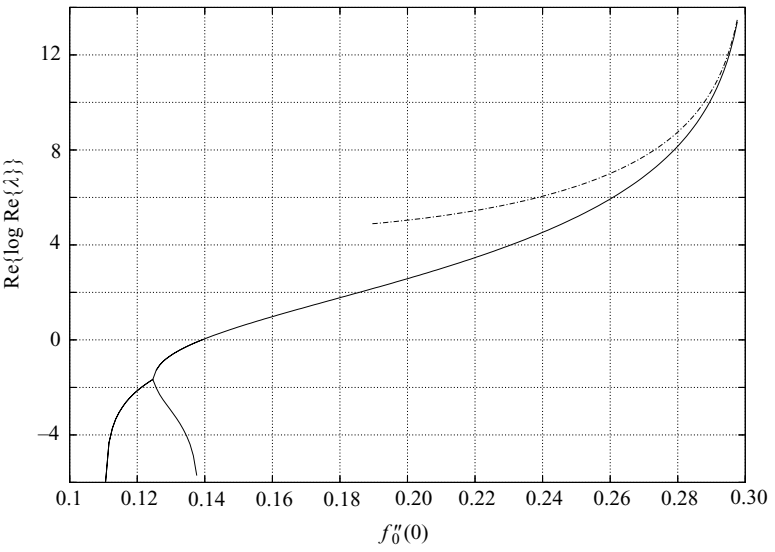

FIGURE 4. The (real part of the) positive eigenvalues for $m = -0.05$ (asymptotic values shown as a broken line).

The second set of eigenvalue distributions is shown in figure 4, and corresponds to the case $m = -0.05$. This distribution replicates most of the features observed in the previous ($m = 0$) case, although there is one slight exception, namely that a second real and positive eigenvalue is also present over a range of values of $f_0''(0)$. This second eigenvalue intersects with the original eigenvalue at $f_0''(0) = 0.125\ldots$, $G_0 = -0.0124\ldots$ to form a complex-conjugate pair of eigenvalues (which extends from this point to smaller values of $f_0''(0)$ – this is the left-hand branch on figure 4). It should be noted that in the context of non-modal disturbances, complex eigenvalues are quite rare. As in the previous case at the point where $f_0''(0) = 0-$, a (probable) infinite number of positive eigenvalues spontaneously appear.

The next set of results presented (figure 5) is for $m = 0.2$. Although in this case the vast majority of eigenvalues appeared to be real (again), the results are intriguingly qualitatively different from the results for the previous two choices of m. When $m = 0.2$, although the unboundedness in λ as $G_0 \to 0-$ is clearly present again (this mode terminating with $\lambda = 0$ at the nose of the distribution curve, figure 1), in this case as G_0 is reduced, additional ($\lambda > 0$) modes form, arising with infinite magnitude at other (negative) values of G_0. Figure 5 shows the first four modes found; many others appeared to arise at progressively more negative values of G_0. In the limit of $\lambda \to \infty$ these computations became quite challenging, and the results shown were obtained with an η-grid size of approximately 4×10^{-5} (these results were also checked against control computations with double this grid size). The asymptotic analysis presented later in this section reveals just why such small grid sizes were necessary in this limit. Many other calculations were performed by the authors (but not presented here), and these all pointed to the existence of many modes provided $m > 0$ in the region $G_0 < 0$.

From these results, it is quite clear that there are two (distinct) limits leading to $\lambda \to \infty$: the first as $G_0 \to 0-$, the second at discrete, non-zero critical values of G_0 (which seem to occur only for $m > 0$); these two limits are now considered in §§ 3.1 and 3.2 respectively. Both these limits are important physically, since both correspond to flow disturbances with diminishingly small wavelengths, a theme which

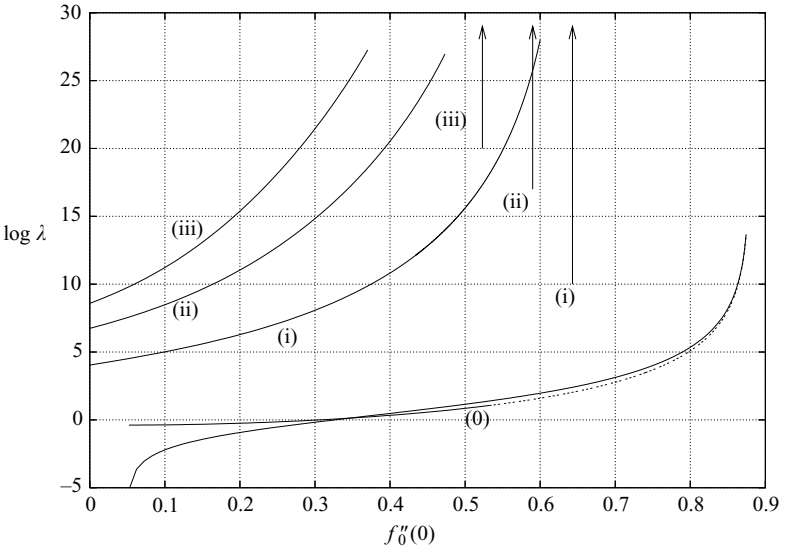

FIGURE 5. The positive eigenvalues for $m = 0.2$ (asymptotic values/locations shown as broken line/arrows).

runs throughout this paper, including in later sections where non-similarity forms of base flow are studied.

3.1. *The large-λ limit, $G_0 \to 0$*

The results presented in figures 3–5 strongly suggest that in the limit $G_0 \to 0-$ one positive eigenvalue becomes unbounded. We now consider this (large-λ) limit. It proves convenient to work with λ as a large parameter and so we pose the ansatz $G_0 = \hat{G}\lambda^{-1/3}$, which may be confirmed *a posteriori*. Inspection of the disturbance equations (3.3) suggests that in this limit the flow will develop a two-tiered structure comprising an inviscid 'core flow', which occupies the majority of the boundary layer, together with a viscous wall layer in which the flow adjusts to the full no-slip boundary conditions.

Standard asymptotic procedures indicate that the solution may be expanded in reciprocal powers of $\lambda^{1/3}$. Thus, for the basic boundary-layer flow we write

$$(f_0, g_0, q_0) = (f_{00}, g_{00}, q_{00}) + \lambda^{-1/3}(f_{01}, g_{01}, q_{01}) + O\left(\lambda^{-2/3}\right), \tag{3.5}$$

where subscript '00' indicates base-flow quantities when $G_0 = 0$. We note that as $\eta \to 0$,

$$f_{00} = \tfrac{1}{2} f_{00}''(0)\eta^2 + \cdots, \quad g_{00} = 1 + g_{00}'(0)\eta + \cdots,$$

where $f_{00}''(0)$ and $g_{00}'(0)$ are the shear and temperature gradient at the surface, respectively.

For $\eta = O(1)$ we expand the disturbance field as

$$(f_1, g_1, q_1) = (f_{10}, g_{10}, q_{10}) + \lambda^{-1/3}(f_{11}, g_{11}, q_{11}) + O\left(\lambda^{-2/3}\right). \tag{3.6}$$

Substituting these expansions into (3.3) gives the solution

$$f_{10} = C f_{00}', \qquad g_{10} = C g_{00}', \qquad q_{10} = \sqrt{2} C g_{00}, \tag{3.7}$$

where we have made use of the far-field boundary conditions (3.4b) on the disturbance quantities. At next order we have

$$f'_{00}f'_{11} + f'_{01}f'_{10} - f''_{00}f_{11} - f_{10}f''_{01} = -\hat{G}q_{10}. \tag{3.8}$$

In order to correctly define the matching condition for the viscous-layer region (to be considered subsequently) we require the limiting behaviour of f_{11} as $\eta \to 0$. This is most readily obtained by setting $\eta = 0$ in (3.8) to give

$$f''_{00}f_{11} = \hat{G}q_{10} \quad \text{on} \quad \eta = 0. \tag{3.9}$$

We then have

$$f_{11}(0) = \frac{\sqrt{2}C\hat{G}}{f''_{00}(0)}. \tag{3.10}$$

Combining this result with the leading-order solution in the core we find that, as $\eta \to 0$, the core flow behaves as

$$f_1 = Cf''_{00}(0)\eta + \frac{\sqrt{2}C\hat{G}}{f''_{00}(0)}\lambda^{-1/3} + \cdots. \tag{3.11}$$

The solution given above does not satisfy the full no-slip boundary conditions on $\eta = 0$. We must therefore introduce a thin viscous layer to enable the disturbance amplitude to adjust from its constant level as it exits the core to a zero value on the plate surface. By balancing normal diffusion with streamwise advection in the sublayer, we are led to conclude that $\eta = \lambda^{-1/3}z$, $z = O(1)$ is the appropriate scaling, and subsequently that in the viscous layer, the disturbance quantities expand as

$$f_1 = \lambda^{-1/3}\hat{f}_1 + \cdots, \qquad g_1 = \hat{g}_1 + \cdots, \qquad q_1 = \hat{q}_1 + \cdots. \tag{3.12}$$

Substitution of these expansions into (3.3) gives, to leading order

$$\hat{f}_{zzz} - 2f''_{00}(0)z\hat{f}_z + 2f''_{00}(0)\hat{f} = 2\sqrt{2}\hat{G}, \tag{3.13}$$

where we have defined $\hat{f}_1 = C\hat{f}$. The boundary conditions on $\hat{f}$ are

$$\hat{f} = \hat{f}_z = 0 \quad \text{on} \quad z = 0, \tag{3.14a}$$

and

$$\hat{f} \to f''_{00}(0)z + \frac{\sqrt{2}\hat{G}}{f''_{00}(0)} + \ldots \quad \text{as} \quad z \to \infty. \tag{3.14b}$$

Integrating (3.13) and applying the wall boundary conditions (3.14*a*) gives

$$\hat{f} = A\int_0^z \int_0^t \mathrm{Ai}\big((2f''_{00}(0))^{1/3}s\big)\,\mathrm{d}s\,\mathrm{d}t, \tag{3.15}$$

where A is a constant of integration. Matching with the core flow then yields

$$A = 3f''_{00}(0)(2f''_{00}(0))^{1/3}, \qquad \hat{G} = \frac{3}{2^{5/6}}f''_{00}(0)^{5/3}\mathrm{Ai}'(0). \tag{3.16}$$

Noting that $\mathrm{Ai}'(0) < 0$, we therefore find that for $G_0 < 0$ the flow supports disturbances which grow algebraically. Confirmation of the consistency, as $G_0 \to 0$, between the (fully) numerical results obtained for (3.3) and the asymptotic results obtained above may be seen on figures 3–5, the latter being indicated by broken lines on these figures.

3.2. *The large-λ limit, $G_0 \to G_0^{crit} \neq 0$*

In addition to the mode with eigenvalue that originates and becomes unbounded as $G_0 \to 0-$, the results for free-stream-flow parameter $m = 0.2$, as shown in figure 5, exhibit additional downstream-growing modes, which form at finite values of $G_0 = G_0^{crit}$, also with unbounded values of λ. The details of the formation of these modes, as $G_0 \to G_0^{crit}$ are quite different from those described in § 3.1, and we study this aspect next.

As before, it is useful to consider the eigenvalue λ as our large parameter, and then to write

$$G_0 = G_0^{crit} + \lambda^{-1/3}\hat{G} + \cdots, \tag{3.17}$$

where the scaling on λ may (again) be verified *a posteriori*. Usefully, the expansions (3.5) and (3.6) are again appropriate (although now the subscript 00 indicates base-flow quantities evaluated at $G_0 = G_0^{crit}$), and when substituted into (3.3), the largest (powers of λ) terms yield

$$f'_{00}f''_{10} + \left[\frac{\sqrt{2}G_0^{crit}g'_{00}}{f'_{00}} - f'''_{00}\right]f_{10} = 0. \tag{3.18}$$

Since this equation is fundamentally inviscid in nature, the appropriate boundary conditions are that

$$f_{10}(0) = 0, \quad f'_{10}(\eta \to \infty) \to 0. \tag{3.19}$$

However, the system (3.18) taken together with (3.19) is a homogeneous one. Consequently the authors tackled the system as an eigenvalue problem (for G_0^{crit}), and then accepted the solution if the calculated value of G_0^{crit} and the actual value of G_0, used in calculating the base flow, coincided. More specific details regarding this will be given below when we discuss our results.

It is useful to be rather more precise regarding the behaviour of f_{10} as $\eta \to 0$. A Frobenius-type expansion of f_{10} reveals that the two linearly independent solutions close to $\eta = 0$ take the form

$$f_{10} \sim A_-\eta^{\Lambda_-} + A_+\eta^{\Lambda_+}, \tag{3.20}$$

where

$$\Lambda_\pm = \frac{1}{2} \pm \frac{1}{2}\left[1 - \frac{4\sqrt{2}G_0^{crit}g'_{00}(0)}{f''_{00}(0)^2}\right]^{1/2}. \tag{3.21}$$

Since in the case when $m = 0$, $g'_{00}(0) = 0$, these values are 0 (which must be discarded) and 1, then it is immediately clear why these types of mode are not present when $m = 0$. Inspection of the numerical results presented above (and many others obtained by the authors) in fact indicated that the pertinent range corresponded to the regime for which $4\sqrt{2}G_0^{crit}g'_{00}(0)/(f''_{00}(0)^2) > 1$, and hence the $\Lambda_\pm$ formed a complex-conjugate pair (along with the $A_\pm$). There must clearly be a sublayer that forms on $\eta = 0$. It turns out (again) that $\eta = \lambda^{-1/3}z$ is the appropriate scaling, although to leading order this layer plays a passive role.

We now consider some numerical results for this particular limit, focusing our attention on the predicted critical values of G_0 for which these very short-wavelength disturbances appear, i.e. the values of G_0^{crit}. As already mentioned, the system (3.18) together with (3.19) may be regarded as an eigenvalue problem for G_0^{crit}, which in our case is only meaningful when G_0^{crit} and the G_0 corresponding to the basic-flow solution coincide. To tackle this problem a value of G_0 was assumed, the basic flow computed

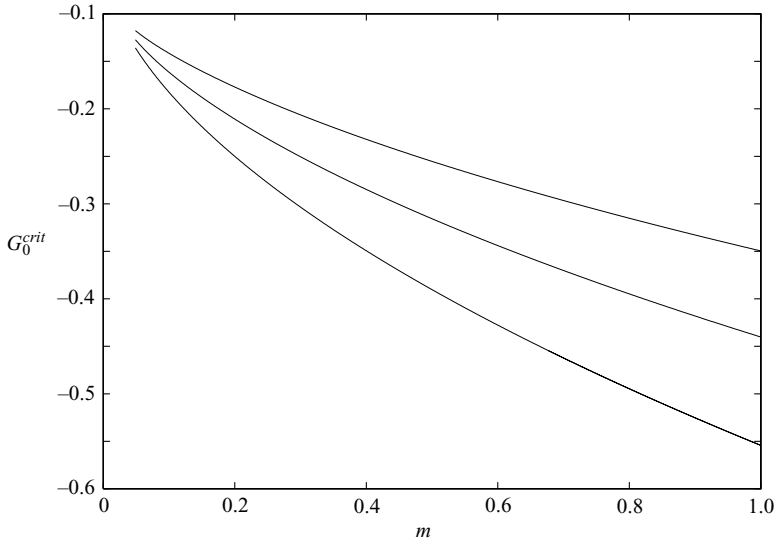

FIGURE 6. Variation of G_0^{crit} with m, first three modes.

(in the manner described earlier in this section), and then (3.18) was approximated using second-order finite differences. A QZ algorithm was adopted to obtain first estimates for G_0^{crit}, and these were then refined using smaller grid sizes in a local search algorithm, which employed a Newton iteration procedure to adjust the value of G_0 to coincide with G_0^{crit} (to within some prescribed tolerance). Typically, exceedingly small grid sizes were again found to be necessary to achieve graphical accuracy – generally $O(5 \times 10^{-7})$; the reason for this is not surprising, given the asymptotic behaviour as $\eta \to 0$ described by (3.20)–(3.21), which indicates decreasingly short-wavelength oscillations in the η-direction in this limit. Figure 6 shows the variation of the first three modes (i.e. G_0^{crit}) of this type over a range of values of m. Indeed, the indications were that many modes are encountered (again, provided $m > 0$). For comparison, the arrows on figure 5 indicate the location of the corresponding critical values of $f_0''(0)$ (for the particular case $m = 0$) for these three modes (labelled (i)–(iii)). Additional evidence of the multiplicity of modes is provided in figure 7, which rather than using an iterative-type procedure to determine the critical values of G_0/G_0^{crit}, shows the minimum difference between G_0 and any of the G_0^{crit} which were computed using the QZ procedure. The significance of these results is that any zeros of the quantity $G_0^{crit} - G_0$ indicate values of G_0 where (infinite) modes originate. These results (which are for the case $m = 0.2$) show vividly that more and more modes appear as the critical location where $f_{00}''(0) = 0$ is approached (from the positive $f_{00}''(0)$ side), the implication being that an infinite number of these modes exist (i.e. a continuous spectrum) in this limit. Unsurprisingly, iterative procedures tend to fail in this regime.

Yet further credence can be given here to the multiplicity of modes by additional asymptotic analysis. Let us assume that $G_0 = G_{00} - \tilde{G}$, where $\tilde{G} > 0$, $|\tilde{G}| \ll 1$ and G_{00} is the value of G_0 for which $f_{00}''(0) = 0$; this anticipates explicitly that this regime is between the nose of the distributions shown in figure 1, and the point of flow reversal.

We now define a scaled transverse coordinate, $\hat{\eta} = \eta/\tilde{Q}$, and so (3.18) becomes

$$\frac{\mathrm{d}^2 f_{10}}{\mathrm{d}^2\hat{\eta}^2} + \frac{1}{\tilde{G}^2}\left(\frac{\sqrt{2}G_{00}g_{00}'(\eta = 0; G_0 = G_{00})}{\left[\frac{1}{2}f_{00}'''(\eta = 0; G_0 = G_{00})\hat{\eta}^2 + \kappa\hat{\eta}\right]^2}\right) f_{11} = 0, \tag{3.22}$$

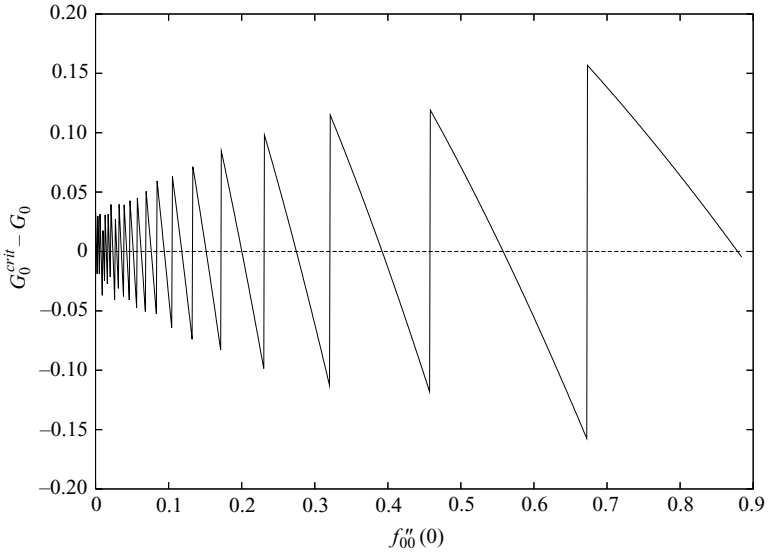

FIGURE 7. $G_0^{crit} - G_0$, $m = 0.2$ ($\Delta\eta = 0.000833$).

where

$$\kappa = -\frac{\partial^3 f_{11}}{\partial^2 \eta \partial G_0}(\eta = 0, G_0 = G_{00}) > 0. \tag{3.23}$$

Usefully, this equation has an exact solution which may be written in the form

$$f_{11} = B_1 \hat{\eta}^{r_1} \left[\tfrac{1}{2} f_{00}'''(\eta = 0; G_0 = G_{00}) + \kappa \hat{\eta}\right]^{1-r_1} + B_2 \hat{\eta}^{r_2} \left[\tfrac{1}{2} f_{00}'''(\eta = 0; G_0 = G_{00}) + \kappa \hat{\eta}\right]^{1-r_2}, \tag{3.24}$$

where r_1, r_2 are the two roots of the equation

$$r(r-1) + \frac{4\sqrt{2} G_{00} g'(\eta = 0; G_0 = G_{00})}{\tilde{G}^2 f_{00}'''(\eta = 0; G_0 = G_{00})^2} = 0. \tag{3.25}$$

The key points to note from this, therefore, are that (3.24) satisfies the wall condition (impermeability) for all values of B_1 and B_2 whilst as $\eta \to \infty$, $f_{11} \sim \text{constant} \times \hat{\eta}$, strongly pointing to the fact that potential solutions exist for all (positive) values of $\tilde{G}$, confirming our assertion that a continuous spectrum of modes exists as $G_0 \to G_{00}$.

Finally (with respect to these inviscid modes), note that the above analysis predicts just the location of the origin of these modes; calculation of the asymptotic value of the corresponding eigenvalues requires higher-order analysis, which is omitted in the interests of brevity.

4. The non-parallel evolution of the boundary layer

We now turn our attention to the question of the non-parallel development of the buoyant boundary layer. In particular we focus our attention on the question of how the boundary layer responds when the wall temperature is variable (or more precisely, decreases with distance downstream from the leading edge of the plate). Our initial interest in this problem arose because of a desire to understand the phenomenon of velocity overshoot in buoyant mixed forced–free convection boundary layers and whether this overshoot could be controlled through a judicious

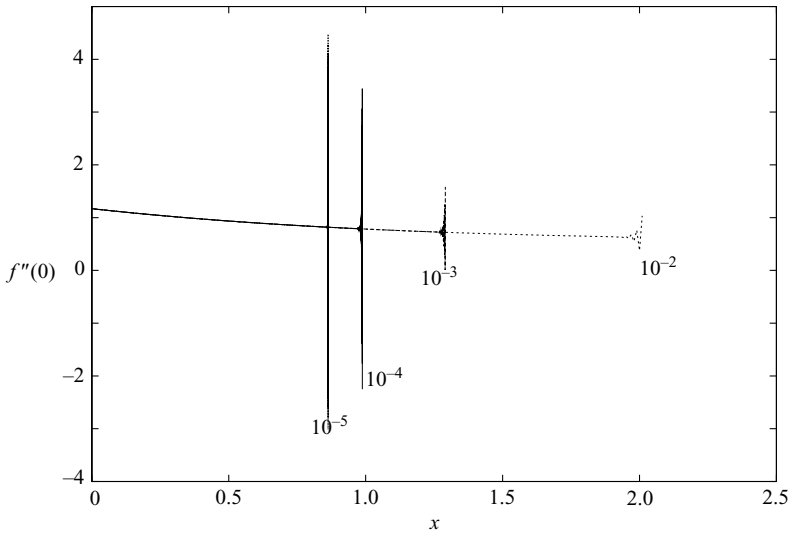

FIGURE 8. Spatial development of wall-shear stress, $m = 0$, $G_0 = 0.5$, $\gamma = -0.1$, Δx as shown.

choice of wall temperature. The development of overshoot is intimately linked with the generation of short-wave instabilities in this class of boundary-layer flow (see Denier & Mureithi 1996; Mureithi *et al.* 1997; Denier & Bassom 2003).

In order to tackle the question of spatially developing (i.e. non-self-similar) flows, we revert to a consideration of the system (2.6)–(2.8). The self-similarity is broken by the choice of a downstream-varying wall temperature as

$$T_w(x) = \mathrm{e}^{-x} + \gamma(1 - \mathrm{e}^{-x}), \tag{4.1}$$

where here γ is treated as a parameter, controlling the downstream evolution of the flow. Consistent with the form (4.1), the initial profiles at $x = 0$ may be taken as the similarity solutions obtained from (3.1). A second-order finite-difference/Crank–Nicolson scheme (coupled with Newton iteration) was then employed to march the solution downstream.

Figure 8 shows the downstream development of the wall-shear stress ($f''(\eta = 0)$), for the case $m = 0$, $\gamma = -0.1$, $G_0 = 0.5$. These results were obtained using four streamwise grid sizes, namely $\Delta x = 10^{-2}$, 10^{-3}, 10^{-4} and 10^{-5} (for a fixed transverse grid size, $\Delta\eta = 5 \times 10^{-3}$). It is immediately apparent that these results suffer a spontaneous breakdown, characterized by sudden oscillations (which on close inspection are of a streamwise point-to-point nature). Other flow quantities (e.g. the wall temperature gradient) exhibited the same type of behaviour. The genesis of this is highly grid dependent. There is clearly no sign of flow reversal occurring, nor of any other 'suspicious' base-flow behaviour immediately prior to this event. It should be noted that for the choice of the parameters taken, there does (in principle) exist a far downstream solution, that is with $m = 0$, $G_0 = 0.5$, $T_w = -0.1$ (which, by rescaling the temperature, is equivalent to $G_0 = -0.05$, $T_w = 1$).

A second example is presented in figure 9; the parameters taken correspond to those of figure 8, but with $\gamma = 0.1$; again, results are presented for a variety of streamwise step sizes, and are qualitatively similar to the previous set of results, exhibiting a sudden breakdown at locations which are again highly dependent upon grid size. An important matter of detail here is that (again) for this regime a far downstream

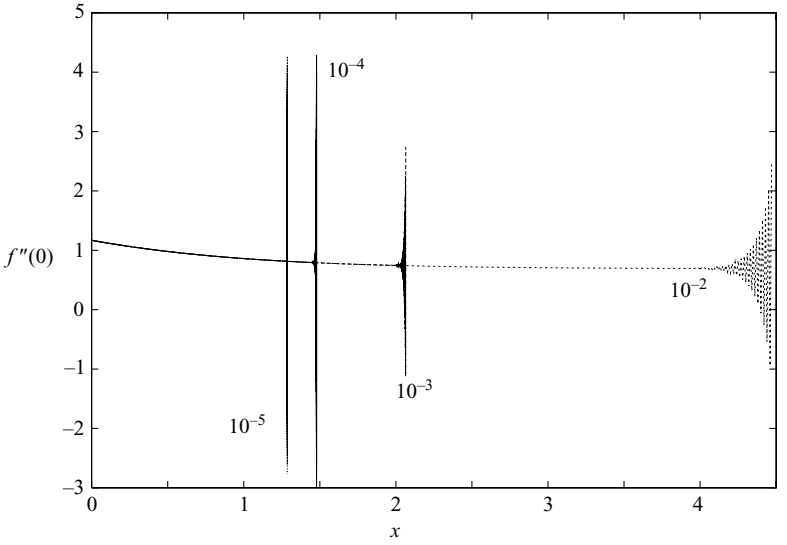

FIGURE 9. Spatial development of wall-shear stress, $m = 0$, $G_0 = 0.5$, $\gamma = 0.1$, Δx as shown.

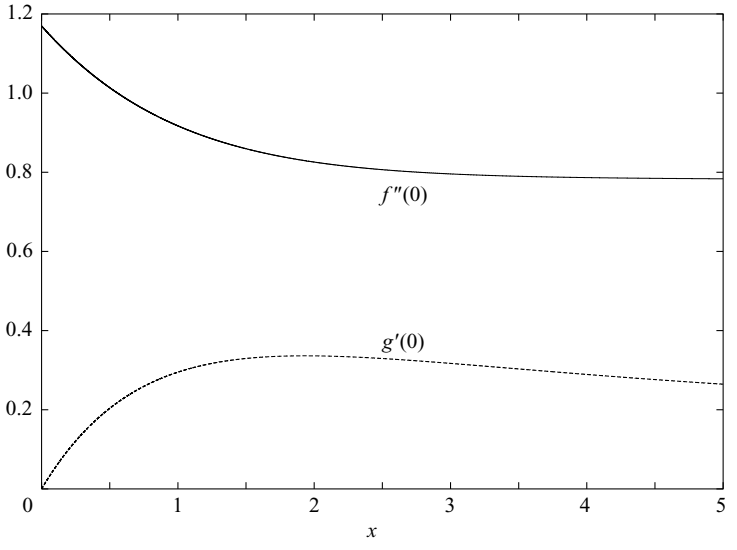

FIGURE 10. Spatial development of wall-shear stress and wall temperature gradient, $m = 0$, $G_0 = 0.5$, $\gamma = 0.25$.

solution does exist, equivalent to the similarity form corresponding to (with rescaling) $T_w = 1$, $G_0 = 0.05$, implying that such failures can occur, even with the local equivalent of positive values of the Grashof number far downstream.

A final example involving the marching procedure is provided in figure 10; again, all parameters remain unchanged from the previous two examples, except in this case $\gamma = 0.25$. Here the solution proceeds downstream, unabated, with the far-downstream form being (asymptotically) approached. It is clear that this case differs significantly from the previous two examples in which the spontaneous breakdown in the calculation was observed.

In order to investigate the difficulties encountered in the cases $\gamma = 0.1$ and -0.1 a procedure closely analogous to that developed for the similarity states was adopted, namely one based on (3.2). Here we seek local solutions of the form

$$(f, g, q) = (f_0(\eta; x), g_0(\eta; x), q_0(\eta; x)) + \epsilon(f_1(\eta; x), g_1(\eta; x), q_1(\eta; x)) \exp \Theta(x) + O(\epsilon^2), \tag{4.2}$$

where the amplitude ϵ is assumed small.

From the onset it must be stressed that the approach to be adopted here (unlike any of those developed elsewhere in this paper) may be regarded as somewhat heuristic, but nonetheless extremely useful in understanding the difficulties experienced in the numerical marching computations, detailed above, and does become increasingly valid in the short-wavelength limit, $|x\Theta_x| \to \infty$. Taking the $O(\epsilon)$ terms when (4.2) is substituted into (2.6) yields

$$f_1''' + (m+1) f_0 f_1'' - 2(2m + x\Theta_x) f_0' f_1' + (m + 1 + 2x\Theta_x) f_1 f_0'' - G_0(2(2m + x\Theta_x) q_1 + (m-1)\eta q_1') = 2x \left(f_0' \frac{\partial f_1'}{\partial x} + f_1' \frac{\partial f_0'}{\partial x} - f_0'' \frac{\partial f_1}{\partial x} - f_1'' \frac{\partial f_0}{\partial x} \right), \tag{4.3a}$$

$$\frac{1}{\sigma} g_1'' - (5m - 1 + 2x\Theta_x) g_1 f_0' + (m+1) f_0 g_1' + (m + 1 + 2x\Theta_x) f_1 g_0' + (5m - 1) g_0 f_1' = 2x \left(f_0' \frac{\partial g_1}{\partial x} + f_1' \frac{\partial g_0}{\partial x} - g_0' \frac{\partial f_1}{\partial x} - g_1' \frac{\partial f_0}{\partial x} \right), \tag{4.3b}$$

$$q_1' - \sqrt{2} g_1 = 0, \tag{4.3c}$$

subject to (3.3); as before, primes denote differentiation with respect to η. We now make the assertion that both the base flow f_0, g_0, q_0 and perturbation quantities f_1, g_1, q_1 are slowly varying in the streamwise direction, thereby permitting the neglect of the right-hand-side terms in (4.3). If we then write $\lambda = x\Theta_x$, we recover (3.3). This system was solved in precisely the same manner as that employed previously, except the analysis was performed at each streamwise location (i.e. on the corresponding local base flow profile). Results for $\gamma = -0.1$ and 0.1 (corresponding to figures 8 and 9) are shown in figures 11 and 12 respectively. Here we have only shown 'unstable' eigenvalues (as previously, negative eigenvalues are of little importance in this context). It is immediately apparent that in both cases, a large (infinite) eigenvalue forms at a finite downstream location, which therefore suggests that infinitely short-wavelength disturbances are responsible for the numerical marching difficulties experienced with $\gamma = -0.1$ and $\gamma = 0.1$. Similar eigenvalue searching procedures were adopted for the case $\gamma = 0.25$, but these failed to detect any positive values of λ, an observation entirely consistent with the lack of difficulties encountered with the marching scheme in this case.

The conclusion therefore is that in cases where these infinitesimal-wavelength unstable disturbances exist, marching schemes will (inevitably) fail. Indeed, the results shown in figures 11 and 12 clearly indicate that downstream the wavelength of the disturbances increases, and it is therefore entirely reasonable to conclude that these will only be detected by numerical marching schemes when the numerical grid is of sufficient resolution to detect these disturbances. The analysis of § 3.2 suggests that the streamwise step size (Δx) must be at least comparable to the third power of the wavelength of the disturbance, namely $\lambda^{-1/3}$. This fully explains why in figures 8 and 9 the failure is clearly observed at earlier streamwise locations as the numerical grid (Δx) is reduced.

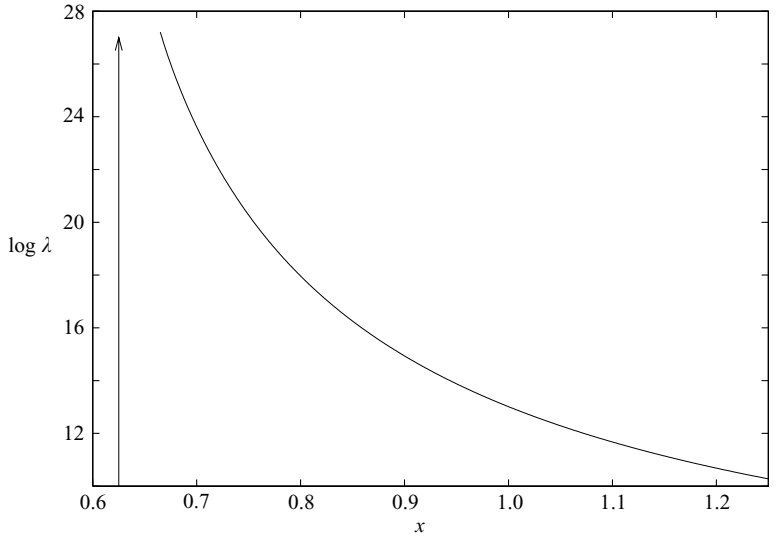

FIGURE 11. Downstream variation of local eigenvalues, $m = 0$, $G_0 = 0.5$, $\gamma = -0.1$.

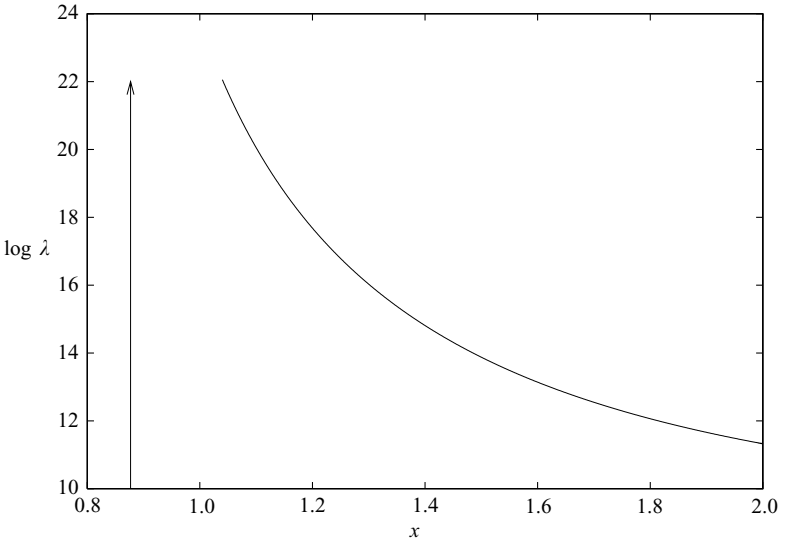

FIGURE 12. Downstream variation of local eigenvalues, $m = 0$, $G_0 = 0.5$, $\gamma = 0.1$.

Returning to a more formal (rational) treatment of the problem, we can make further analytical progress on understanding this phenomenon, guided by the work of § 3.2. Supposing that $\lambda \to \infty$ as $x \to x_0$, then § 3.2 strongly suggests we should seek a disturbance whose wavelength is $O((x - x_0)^3)$, and so in place of (4.2), more formally we write, as $x \to x_0^+$,

$$(f, g, q) = (f_{00}(\eta), g_{00}(\eta), q_{00}(\eta)) + O(x - x_0) + \{(f_{10}(\eta), g_{10}(\eta), q_{10}(\eta)) + O(x - x_0)\} \exp\left\{\frac{-\lambda_0}{(x - x_0)^2}\right\} + \ldots. \quad (4.4)$$

In the core of the flow ($\eta = O(1)$), this leads formally to the system (3.18)–(3.19), where in this case f_{00} is taken to be the local base-flow solution (at $x = x_0$). The system was solved (as before) at each streamwise location, and when the eigenvalue G_0^{crit} corresponded to the actual Grashof number G_0, this location was then deemed to be the point where infinite spatial (λ) eigenvalues appeared, i.e. $x = x_0$. For the cases $\gamma = -0.1$ and 0.1 these locations are clearly marked by vertical arrows on figures 11 and 12 respectively. Inspection of these figures (and indeed of the numerical results in detail) indicate consistency between the numerical results obtained from (4.3) and the predicted origin of these modes (x_0) obtained from (3.18)–(3.19). A sublayer will also be present, which (again, consistent with § 3.2) will be of thickness $\eta = O(x - x_0)$; however to leading order this plays a passive role. Asymptotic predictions for the values of λ requires solution to higher order, which is omitted for brevity.

5. The suppression of the instability

The difficulties associated with the failures of marching schemes are a serious restriction on the usefulness of the procedure. However the problems encountered here have some similarities (and differences) with those found by Duck *et al.* (1999) in which linearly growing eigenfunctions, which were triggered by perturbing algebraically growing eigenfunctions, were observed. There is one extremely important difference between the current difficulties with the marching procedure and those encountered in the Duck *et al.* (1999) paper, insofar as in the cases $\gamma = -0.1, 0.1$, described above, there are no eigenfunctions which spring from the leading edge – rather (infinite) eigenvalues are encountered at finite downstream locations. In Duck *et al.* (1999) the difficulties were overcome by treating the (parabolic) problem as quasi-elliptic, imposing (physically reasonable) downstream as well as upstream boundary conditions. This type of procedure, in the context of parabolic systems, can be justified, insofar as it 'selects' the appropriate eigen-form to give the desired behaviour to the problem downstream. As noted by Duck *et al.* (1999) this type of approach is reminiscent of that adopted in free-interaction/triple-deck work (see Stewartson & Williams (1969), for example, § 6). This is the motivation behind the procedure we adopt here.

The system (2.6) was therefore treated quasi-elliptically. As before, boundary conditions at the leading edge were imposed (using the appropriate similarity solution), whilst Neumann boundary conditions were imposed (at a finite x location) downstream (this treatment worked well in the study of Duck *et al.* (1999) and proved very effective in the present study); this condition is completely consistent with the imposed conditions, notably (4.1), which is expected to lead to a similarity form far downstream. Second-order central differencing was used in both the η- and x-directions. In order to solve the resulting nonlinear set of algebraic equations, Newton iteration was employed, i.e. the entire flow field was calculated simultaneously (the banded nature of the algebraic system was fully exploited which made this possible). A typical calculation involved a streamwise grid size of $\Delta x = 0.025$, a transverse grid size of $\Delta\eta = 0.1$ and no more than five iterations (for convergence to within 10^{-6}).

The first set of results using this quasi-elliptic procedure is shown in figure 13; this corresponds to the case computed earlier with the marching routine, as illustrated in figure 8, namely $\gamma = -0.1$, $G_0 = 0.5$ and $m = 0$. The elliptic-type procedure has no difficulty in computing solutions (which are accurate to within the graphical accuracy of the figures). It is clear that the imposition of (reasonable) downstream conditions

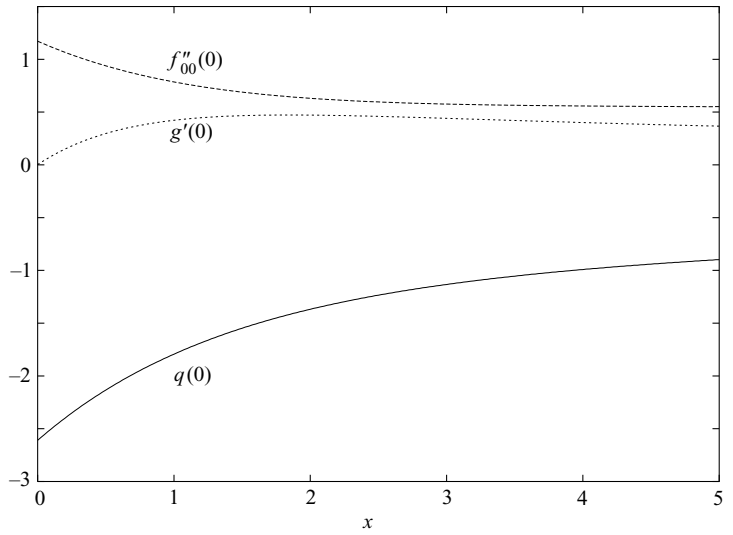

FIGURE 13. Spatial development of wall-quantities, $m = 0$, $G_0 = 0.5$, $\gamma = -0.1$.

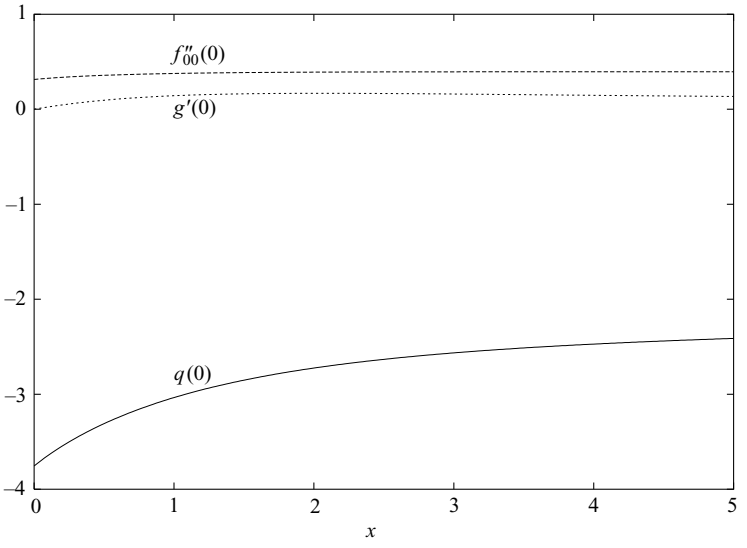

FIGURE 14. Spatial development of wall-quantities, $m = 0$, $G_0 = -0.05$, $\gamma = 0.5$.

leads to a complete suppression of the small-scale instabilities, over which marching schemes have no control. This same procedure also yielded completely regular results for the other 'problematic' case considered in the previous section (figure 9).

The second set of results obtained using this procedure is presented in figure 14, corresponding to the parameter choice $m = 0$, $G_0 = -0.05$, $\gamma = .5$, which corresponds to an example where leading-edge eigenvalues will be present (i.e. immediately at $x = 0$). Again, in spite of the presence of downstream-growing eigensolutions, the quasi-elliptic procedure is able to identify a solution state which extends smoothly downstream (towards another similarity state). The method proved extremely efficient in identifying solutions, provided similarity states existed far downstream.

6. Conclusions

Flows of the type considered in this paper exhibit a number of interesting phenomena, most of which are linked to the occurrence of algebraically growing (in the downstream direction) eigensolutions. Instabilities of this type have received a great deal of attention, recently, in particular with regard to transient growth in boundary layers (Luchini 1996; Andersson *et al.* 1999; Luchini 2000). However there is one important distinction between the current work, and these previous studies, in that as the present problem exhibits algebraic instabilities, even in two-dimensional contexts, whilst in the aforementioned boundary-layer studies, three-dimensionality was an inherent necessity for the occurrence of such modes. In the present study, one requirement is that for the similarity forms to be algebraically unstable, it is necessary for the wall temperature to be lower than that of the free stream, i.e. the requirement is that $G_0 < 0$. Since our results indicate that diminishingly small-wavelength disturbances exist as $G_0 \to 0-$, this suggests that very small amounts of surface cooling could provoke small wavelength disturbances, which could have important practical implications. Indeed, the work of Steinrück (1994) supports this assertion, given that his study was linked to the case $m = 0$, $G_0 = 0-$ (in our notation). It is therefore inevitable that in this case instabilities are present immediately from the leading edge. It is worthy of note that (3.16) and (3.21) do have some similarity to the results of Steinrück (1994), although as noted earlier, the present analysis may be regarded as being somewhat more complete.

In the case of non-similarity flows, the situation is even more intriguing. The results of § 4 clearly reveal the further subtleties associated with flows of this type, especially the occurrence of eigensolutions, which form spontaneously through the formation of essential singularities; these in turn lead to exceedingly challenging numerical tasks. The present work also reveals that heated plates can also be susceptible to these numerical difficulties. However, the quasi-elliptic treatment of the non-self-similar flows bypasses the difficulties associated with the triggering of (very) short-wavelength disturbances; the imposition of downstream boundary conditions appears to render the problem well posed, and this leads to sensible (credible) solutions extending from the leading edge of the plate, to far downstream.

The treatment and procedure adopted in § 5 is similar to those used in free-interaction/(supersonic) triple-deck work over many years (originating from the study of Stewartson & Williams 1969). In these latter types of problems, (again) eigensolutions exist, which in the linear context grow exponentially fast downstream. If allowed to develop into the nonlinear regime, these eigensolutions then lead either to a flow with a pressure increase that leads to separation, or to a flow which undergoes (unbounded) expansion at a point. Over the years, a number of techniques have been developed in order to suppress these instabilities/breakdowns. One technique (e.g. Daniels 1974) involves introducing a small amplitude eigensolution far upstream of any flow perturbation, and adjusting the magnitude of this (iteratively) so that far downstream, the flow asymptotes to some reasonable conditions and also finite-location breakdowns are avoided. A second approach, proposed by Burggraf & Duck (1982) involves Fourier transforming the problem (in the streamwise direction), a technique which automatically handles upstream/downstream issues (implicitly assuming reasonable downstream conditions). A third approach, which has some similarity with the treatment of § 5 was proposed by Rizzetta, Burggraf & Jenson (1978), treating the (interaction) problem in a quasi-elliptic manner, thereby again suppressing exponentially growing eigenstates. All three approaches lead to the same results. It should also be noted that techniques similar to those described above can

be applied to study the effects of a class of three-dimensional disturbance to a wide class of boundary-layer flows (Duck *et al.* 1999). In these latter cases, streamwise algebraically growing eigensolutions exist, similar to those encountered in § 3, but it is possible to find solutions that extend from the leading edge to far downstream, which are bounded and which do not exhibit breakdowns. On the other hand, if the eigensolutions are not suppressed, then Duck (2003) found that either the flow would exhibit an inviscid type of singularity or could make a translation to another base state downstream.

This procedure has been validated experimentally in the context of turbulent boundary layers. The early work of Clauser (1954), which was concerned with the effect of adverse pressure gradients on turbulent boundary layers, demonstrated that in the presence of rather flat pressure distributions the flow developed one particular downstream state. Changes to steeper pressure gradients resulted in a different downstream response. In this case the flow pressure distribution (along the whole wind tunnel) serves to select the downstream response and effectively amounts to prescribing a downstream boundary condition on the flow, just as we have done in our computations. Furthermore, Clauser (1954) demonstrated that small changes to the steeper pressure gradients (made simultaneously at several points) resulted in a flow whose response was 'chaotic'. Clauser (1954) argued that this response indicated that some form of downstream instability was present within the flow. These experimental results are, intriguingly, consistent with our theoretical results. However, we should emphasise that Clauser's experiments are for turbulent boundary layers with no appreciable buoyancy present.

As with the free-interaction problem, it can be argued that both sets of solutions (i.e. those that do not exhibit breakdowns and those that do) are full and proper solutions of the complete equation set. Further, the work of Duck & Dry (2001), which was partly concerned with an initial value approach (both in the streamwise direction and temporally) does suggest that bounded solutions are fully realisable far downstream. Indeed, it is worth re-emphasizing that even the similarity form of the equations can exhibit non-uniqueness over a range of (negative) values of G_0.

A note about the choice of downstream boundary conditions is also in order. For the scenarios considered in § 5, the underlying assumption, which is entirely reasonable from a physical standpoint, is that the flow becomes independent of downstream location (if described in terms of similarity variables), this being consistent with the imposed wall temperature distribution (which itself becomes independent of downstream location). However, it should be possible to devise acceptable downstream conditions for other downstream behaviours, and to incorporate these into the scheme proposed in this paper.

Very short-wavelength disturbances have been observed in a number of viscous flow calculations in the past (see Brinckman & Walker 2001) and it has been suggested (Cowley 2001) that these present a considerable challenge to boundary-layer theory. However it may be that approaches, based on that used in this paper, may be a remedy to such difficulties in other boundary-layer flow situations exhibiting diminishingly small wavelength disturbances.

Parts of this work were completed while P.W.D. was visiting the School of Applied Mathematics at the University of Adelaide. Their kind hospitality is gratefully acknowledged. J.P.D. and J.L. gratefully acknowledge the financial support of the Australian Research Council through grant DP0210877. The authors benefited from a number of useful discussions with Dr R. E. Hewitt.

REFERENCES

Andersson, P., Berggren, M. & Henningson, D. S. 1999 Optimal disturbances and bypass transition in boundary layers. *Phys. Fluids* **11**, 134.

Batchelor, G. K. 1967 *An Introduction to Fluid Dynamics*. Cambridge University Press.

Brinckman, K. W. & Walker, J. D. A. 2001 Instability in a viscous flow driven by streamwise vortices. *J. Fluid Mech.* **432**, 127.

Burggraf, O. R. & Duck, P. W. 1982 Spectral computation of triple-deck flows. In *Numerical and Physical Aspects of Aerodynamic Flows* (ed. T. Cebeci), p. 145. Springer.

Chen, T. S. & Mucoglu, A. 1979 Wave instability of mixed convection flow over a horizontal flat plate. *Intl J. Heat Mass Transfer* **22**, 185.

Clauser, F. H. 1954 Turbulent boundary layers in adverse pressure gradients. *J. Aero. Sci.* **21**, 91.

Cowley, S. J. 2001 Laminar boundary-layer theory: a 20th century paradox? *Proc. ICTAM 2000* (ed. H. Aref & J. W. Phillips), pp. 389–411. Kluwer.

Daniels, P. G. 1974 Numerical and asymptotic solutions for the supersonic flow near the trailing edge of a flat plate. *Q. J. Mech. Appl. Maths* **27**, 175.

Daniels, P. G. 1992 A singularity in thermal boundary-layer flow on a horizontal surface. *J. Fluid Mech.* **242**, 449.

Daniels, P. G. & Gargaro, R. J. 1993 Buoyancy effects in stably stratified horizontal boundary-layer flow. *J. Fluid Mech.* **250**, 233.

Denier, J. P. & Bassom, A. P. 2003 The non-parallel evolution of nonlinear short waves in buoyant boundary layers. *Stud. Appl. Maths* **110**, 139.

Denier, J. P. & Mureithi, E. W. 1996 Weakly nonlinear wave motions in a thermally stratified boundary layer. *J. Fluid Mech.* **315**, 293.

Duck, P. W. 2003 Streamwise algebraic growth (and breakdown) in three-dimensional boundary layers. *Theor. Comput. Fluid Dyn.* **16**, 249.

Duck, P. W. & Dry, S. L. 2001 On a class of unsteady, non-parallel, three-dimensional disturbances to boundary-layer flows. *J. Fluid Mech.* **441**, 31

Duck, P. W., Stow, S. & Dhanak, M. R. 1999 Non-similarity solutions to the corner boundary-layer equations (and the effects of wall transpiration). *J. Fluid Mech.* **400**, 125.

Hady, F. M., Bakier, A. Y. & Gorla, R. S. R. 1996 Mixed convection boundary layer flow on a continuous flat plate with variable viscosity. *Heat Mass Transfer* **31**, 169.

Hartree, D. R. 1937 On an equation occurring in Falkner and Skan's approximate treatment of the equations of the boundary layer. *Proc. Camb. Phil. Soc.* **33**, 223.

Higuerra, F. J. 1992 Linear response of the natural convection boundary layer below a heated horizontal plate. *Eur. J. Mech.* B/*Fluids* **12**, 613.

Hussain, T. & Afzal, N. 1988 Mixed convection boundary layer flow on a horizontal plate in a uniform stream, *Intl J. Heat Mass Transfer* **31**, 2505.

Kumari, M. & Nath, G. 1982 Unsteady mixed convection near the stagnation point in three-dimensional flow. *J. Heat Transfer* **104**, 132.

Leal, L. G. 1973 Combined forced and free convection heat transfer from a horizontal flat plate. *Z. Angew. Math. Mech.* **24**, 20.

Libby, P. A. & Fox, H. 1964 Some perturbation solutions in laminar-boundary layer theory. *J. Fluid Mech.* **17**, 433.

Lin, W. L. & Lin, T. F. 1996 Experimental study of unstable mixed convection of air in a bottom heated horizontal rectangular duct. *Intl J. Heat Mass Transfer* **39**, 1649.

Luchini, P. 1996 Reynolds-number independent instability of the boundary layer over a flat surface. *J. Fluid Mech.* **327**, 101.

Luchini, P. 2000 Reynolds-number-independent instability of the boundary layer over a flat surface: optimal perturbations. *J. Fluid Mech.* **404**, 289.

Mureithi, E. W. 1998 Effects of thermal buoyancy on the stability properties of boundary-layer flows. PhD Thesis, University of New South Wales, Australia.

Mureithi, E. W., Denier, J. P. & Stott, J. A. K. 1997 The effect of buoyancy on upper branch Tollmien–Schlichting waves. *IMA J. Appl. Maths* **58**, 19.

Obrist, D. & Schmid, P. J. 2003 On the linear stability of swept attachment-line boundary layer flow. Part 2. Non-modal effects and receptivity. *J. Fluid Mech.* **493**, 31.

Rizzetta, D. P., Burggraf, O. R. & Jenson, R. 1978 Triple-deck solutions for viscous supersonic and hypersonic flow past corners. *J. Fluid Mech.* **89**, 1978, 535.

Schneider, W. 1979 A similarity solution for combined forced and free convection flow over a horizontal plate. *Intl J. Heat Mass Transfer* **22**, 1401.

Schneider, W. & Wasel, M. G. 1985 Breakdown of the boundary-layer approximation for mixed convection above a horizontal plate. *Intl J. Heat Mass Transfer* **28**, 2307.

Steinrück, H. 1994 Mixed convection over a cooled horizontal plate: non-uniqueness and numerical instabilities of the boundary-layer equations. *J. Fluid Mech.* **278**. 251.

Stewartson, K. & Williams, P. G. 1969 Self-induced separation. *Proc. R. Soc. Lond.* A **312**, 181.

Trefethen, L. N., Trefethen, A. E., Reddy, S. C. & Driscoll, T. A. 1993 Hydrodynamic stability without eigenvalues. *Science* **261**, 578.

Wang, X. A. 1982 An experimental study of mixed, forced, and free convection heat transfer from a horizontal flat plate to air. *J. Heat Transfer* **104**, 139.